

Spiral states in the square-lattice Hubbard model

Sanjoy Sarker

Department of Physics and Astronomy, University of Alabama, Tuscaloosa, Alabama 35487

C. Jayaprakash

Department of Physics, The Ohio State University, Columbus, Ohio 43210

H. R. Krishnamurthy

Department of Physics, Indian Institute of Science, Bangalore 560 012 India

Wolfgang Wenzel

Department of Physics, The Ohio State University, Columbus, Ohio 43210

(Received 27 September 1990)

We present a variety of physical implications of a mean-field theory for spiral spin-density-wave states in the square-lattice Hubbard model for small deviations from half filling. The phase diagram with the paramagnetic metal, two spiral (semimetallic) states, and the ferromagnet is calculated. The momentum distribution function and the (quasiparticle) density of states are discussed. There is a significant broadening of the quasiparticle bands when the antiferromagnetic insulator is doped. The evolution of the Fermi surface and the variation of the plasma frequency and a charge-stiffness constant with U/t and δ are calculated. The connection to results based on the Schwinger-boson-slave-fermion formalism is made.

The possibility of spiral and linear incommensurate spin-density-wave states in doped Heisenberg antiferromagnets (the t - J model and its relatives) and in the Hubbard model has been revived in the context of high- T_c superconductors.¹⁻⁶ A variety of approximate techniques have been used to address this problem. Recently, we proposed a mean-field theory of the Mott-Hubbard metal-insulator transition on nonbipartite lattices⁵ at half filling. Here, we discuss the physical consequences of our theory which accounts for spiral states in the square lattice away from half filling. We have evaluated the momentum distribution function and the quasiparticle density of states in the spiral phase. The quasiparticle bands are narrow at half filling; upon doping, significant expansion of the bands occurs with additional states appearing in the gap region of the insulator and the Fermi energy now lies in these states. We also present results for the plasma frequency determined by the f sum rule and also a charge-stiffness constant studied by Kohn;^{7,8} the latter vanishes in the undoped, insulating phase and its value yields the oscillator strength of the low-frequency part of the f sum rule.

Consider the square-lattice Hubbard model given by

$$H = - \sum_{\langle ij \rangle, \sigma} t (c_{i\sigma}^\dagger c_{j\sigma} + \text{H.c.}) + U \sum_i \hat{n}_{i\uparrow} \hat{n}_{i\downarrow}, \quad (1)$$

where $\langle ij \rangle$ denotes near-neighbor sites and $\hat{n}_{i\uparrow} = c_{i\uparrow}^\dagger c_{i\uparrow}$. We have performed a mean-field analysis of spiral states in the doubly occupied site-state-holon representation. The possibility of linear spin-density waves and charged-spin solitons⁶ will be discussed elsewhere. In fact, for large values of U (in units of t) the spiral states have lower energy than the other states (see below). At half filling we have an antiferromagnetic insulator for all U . Our results for the phase diagram at small deviations from half filling

are as follows: At small values of U the system is in a paramagnetic metallic phase. At U_{c1} , there is a Hartree-Fock instability into an incommensurate spiral state with \mathbf{Q} along the zone boundary $\mathbf{Q} = (q, \pi)$ or (π, q) . At a higher value of $U = U_{c2}$ there is a transition into a spiral state along the (1,1) direction, in agreement with our calculations based on a Schwinger-boson-slave-fermion formalism.^{3,9} At very large U the system goes into a ferromagnetic state in agreement with Nagaoka's results.¹⁰ We have established the existence of the (1,1) spiral and the ferromagnetic phases analytically within a $1/U$ expansion of the Hartree-Fock equations. The momentum distribution function yields a Fermi surface that is very anisotropic for intermediate U but becomes less so at larger values.

We first perform a particle-hole transformation on the spin-up electrons and redefine the operators by $c_{i\uparrow} \rightarrow h_i^\dagger$ and $c_{i\downarrow}^\dagger \rightarrow d_i^\dagger$. With respect to a reference vacuum state $|\Omega\rangle$ that has a spin-up particle at every site, h_i^\dagger creates a holon and d_i^\dagger , a doubly occupied site state at site i . The Hamiltonian in this representation assumes the form

$$H = t \sum_{ij} h_i^\dagger h_j - t \sum_{ij} d_i^\dagger d_j + U \sum_i d_i^\dagger d_i - U \sum_i d_i^\dagger d_i h_i^\dagger h_i. \quad (2)$$

Note that the holons and doubly occupied site states have an attractive on-site interaction leading to an instability toward pairing at a nonzero center-of-mass momentum \mathbf{Q} . A coherent Bose condensation of holon-doubly occupied site-state pairs into a single wave vector \mathbf{Q} corresponds to an xy -spiral spin-density wave with long-range order, with the order parameter $\langle d_i^\dagger h_i^\dagger \rangle = \langle S_i^- \rangle = b_0 e^{i\mathbf{Q} \cdot \mathbf{r}_i}$, where b_0 is the condensate density of the spiral magnetization. The spiral state which is uniformly charged has the advantage that the diagonalization of the quadratic Hamiltonian that results from the Hartree-Fock factorization can be

performed analytically. Other condensates require extensive numerical calculations. We have carried out numerical diagonalization on lattices as large as 40×40 and find that at $\delta=0.1$ and for $U > 12t$ uniformly charged spiral states have lower energy than a state with charged solitons separating antiferromagnetic domains. For intermediate U , preliminary investigations show that allowing the spin configuration of the domains to spiral lowers the energy with respect to the antiferromagnetic soliton state while the pure-spiral state is higher in energy. In this paper we confine our attention to states in which the charge is uniform and only spiral states need be considered.

Spiral states can be described by factorizing the quartic Coulomb term allowing for the corresponding order parameter. We obtain the quadratic mean-field Hamiltonian displayed below:

$$H_{MF} = \sum_{\mathbf{k}} (-t_{\mathbf{k}} - \bar{\mu}) d_{\mathbf{k}}^{\dagger} d_{\mathbf{k}} + \sum_{\mathbf{k}} (t_{\mathbf{Q}-\mathbf{k}} + \bar{\mu}) h_{\mathbf{Q}-\mathbf{k}}^{\dagger} h_{\mathbf{Q}-\mathbf{k}} + Ub_0 \left[\sum_{\mathbf{k}} d_{\mathbf{k}} h_{\mathbf{Q}-\mathbf{k}} + \text{H.c.} \right], \quad (3)$$

where $\bar{\mu}$ is a renormalized chemical potential. A unitary transformation yields the quasiparticle dispersion relations for holons and doubly occupied site states $E_{0\mathbf{k}}, E_{2\mathbf{k}} = R_{\mathbf{k}} \pm [\bar{\mu} + (t_{\mathbf{Q}-\mathbf{k}} + t_{\mathbf{k}})/2]$, where

$$R_{\mathbf{k}} = \{[(t_{\mathbf{Q}-\mathbf{k}} - t_{\mathbf{k}})/2]^2 + (Ub_0)^2\}^{1/2}.$$

In terms of the original degrees of freedom, one has the lower and upper spiral Hubbard bands and the holon (doubly occupied site-state) quasiparticles are merely holes (particles) in the lower (upper) bands. The self-consistent equations which determine the spiral magnetization b_0 and the chemical potential μ_0 can be derived easily. The mean-field energy is minimized with respect to the condensate wave vector \mathbf{Q} and b_0 .

For small values $\delta (\neq 0)$, the wave-vector-dependent susceptibility $\chi(\mathbf{Q})$ for the $U=0$ Hubbard model on a square lattice displays a peak at $(\pm Q, \pi)$ and $(\pi, \pm Q)$ as noted, for example, in Ref. 6. We have verified that at larger deviations from half filling the peak moves first along the zone boundary and then toward $(0,0)$ along $(0, Q)$ at large δ . The spiral instability occurs at $U_{c1} = \chi^{-1}(\mathbf{Q}^*) \propto [\ln(\delta)]^2$ for small δ . We have performed a detailed numerical solution of the self-consistent equations for $U > U_{c1}$ and minimized the energy with respect to the ordering wave vector. An accurate determination of the variation of the energy with the wave vector around the minimum involves a careful numerical evaluation of the Brillouin-zone integrals. These computations lead to the phase diagram displayed in Fig. 1. For fixed filling, as one increases U the paramagnetic phase loses stability to an incommensurate spiral with ordering wave vector (Q_1, π) at U_{c1} . As U increases, Q_1 moves away from the zone corner and at U_{c2} there is first-order transition (on an energy scale of $10^{-4}t$) into a spiral phase with \mathbf{Q} along the diagonal; diagonally incommensurate order facilitates hole motion, thus allowing greater gain in the kinetic-energy term which begins to predominate over the magnetic term at larger values of U . As U is increased, the ordering wave vector moves along the diagonal toward zero. At large U there is a *continuous*

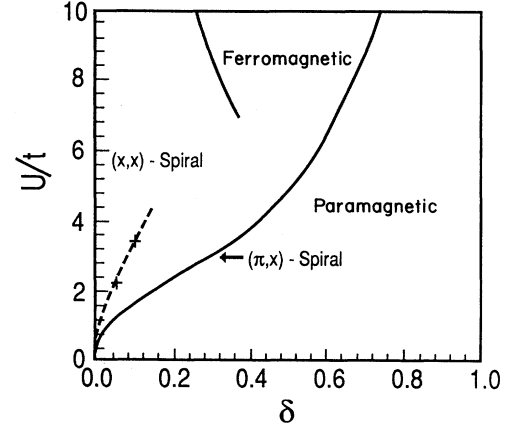


FIG. 1. The phase diagram in the U/t - δ plane showing the paramagnetic, ferromagnetic, and spiral $[(Q, Q)$ and (Q_1, π)] phases. See text for discussion.

transition into a ferromagnetic state as in the analysis based on the Schwinger-boson-slave-fermion formalism.^{3,9}

We have studied the large- U , small- δ behavior analytically. By expanding in powers of t/U the self-consistent equations can be analyzed to yield the sublattice magnetization $b_0 = (1 - \delta)/2 + O(t^2/U^2)$; this result is obvious since quantum fluctuations are not included in the treatment of magnetic ordering. The energy for the diagonal spiral is given by $-2v - 2\delta^2/v$ where $v = t/(Ub_0)$ while that for the ferromagnetic state is $-4\delta + 2\pi\delta^2$. Therefore, the phase boundary between the spiral phase and the ferromagnetic phase occurs at $v_c = \delta(1 - \pi\delta/2)/(1 - 2\pi\delta^2)$. At large U the diagonal spiral is energetically favored over the spiral with the wave vector at (Q_1, π) which has an energy $-2v - \delta^2/v$. The transition between the spiral phase and the ferromagnetic phase is continuous. These analytic results agree with the numerical computations. The large- U part of the phase diagram and the dependence on δ of the spiral wave vector, etc. are in semiquantitative agreement with results from a mean-field theory based on Schwinger bosons and slave fermions for the $t-J$ model³ and for the Hubbard model.⁹ The latter theory, however, does not give rise to the spiral along (Q_1, π) at smaller U obtained in this paper: The Schwinger-boson representation incorporates charge-spin separation, a phenomenon likely to occur only at moderate to large values of U .¹²

We have also calculated the momentum distribution function $n_{\mathbf{k}} = \langle c_{\mathbf{k}\sigma}^{\dagger} c_{\mathbf{k}\sigma} \rangle$ by reexpressing it in terms of the quasiparticle operators that diagonalize the mean-field Hamiltonian. The discontinuity in $n_{\mathbf{k}}$ defines the Fermi surface. The Fermi surfaces for $\delta=0.05$, $U=8$ and $\delta=0.10$, $U=15$ are shown in Fig. 2(a) for the diagonal spiral. Note that for intermediate U , the Fermi surface is very anisotropic but becomes less so as U increases. This is also confirmed by a calculation of the effective-mass tensor at the bottom of the hole band. The principal directions are along the $(1,1)$ direction and perpendicular to it. At $U=8.0$ and $\delta=0.05$ the ratio of the masses is 6.6 while at $U=15$ and $\delta=0.1$ it is about 1.6. For the spiral

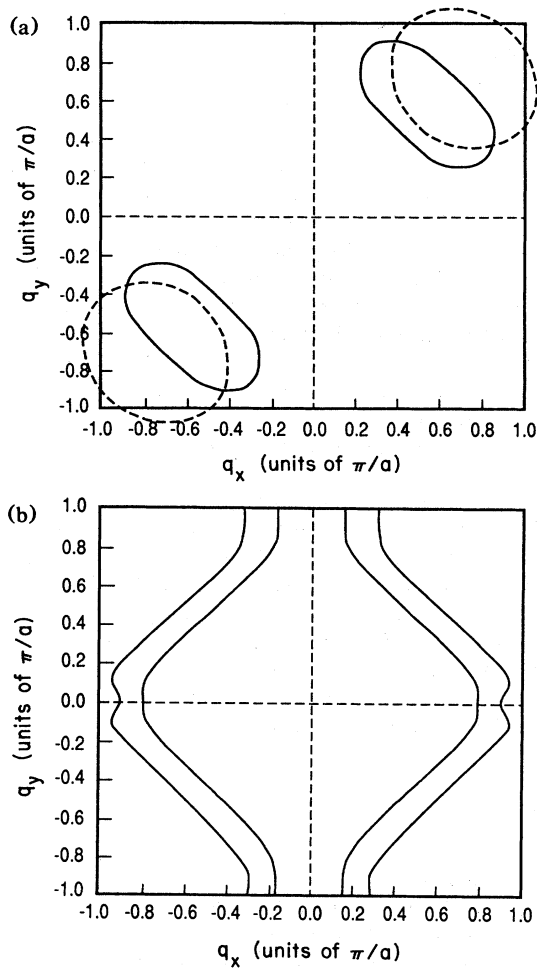


FIG. 2. The quasiparticle Fermi surface in the spiral phase. For the diagonal spiral the dashed line is for $U=8$ and $\delta=0.05$, and the solid line is for $U=15$ and $\delta=0.1$ in (a). In (b) the Fermi surface at $U=3.5$, $\delta=0.1$ for the spiral wave vector $(0.87, 1)$ in units of π is shown.

phase with pitch along (Q_1, π) , the Fermi surface is displayed in Fig. 2(b). Note that in contrast to the diagonal case the Fermi surface is now composed of disjoint curves; this will lead to distinctive signals in de Haas-van Alphen measurements and in magnetoresistance.

In Fig. 3 we have plotted the quasiparticle density of states for the diagonal spiral at $U=15$. There is significant broadening of the bands as the system is doped with holes. At zero doping the width of the band is given by $8t^2/Ub_0$, i.e., of the order of J . The width increases nonlinearly with deviation from half filling and becomes of order t ; the Fermi energy shifts upward by a corresponding amount. Numerically, for $U=15$ the width is approximately t for $\delta=0$ and at $\delta=0.1$ is about 4.9 times larger. In fact, the gap between the bands decreases by about half as it gets partially filled by states from above and below. The Fermi surface in the doped case lies in the insulating gap. These features are in rough accord with data from recent photoemission experiments.¹³ We stress that the shifting of Q from the zone corner is essential for this

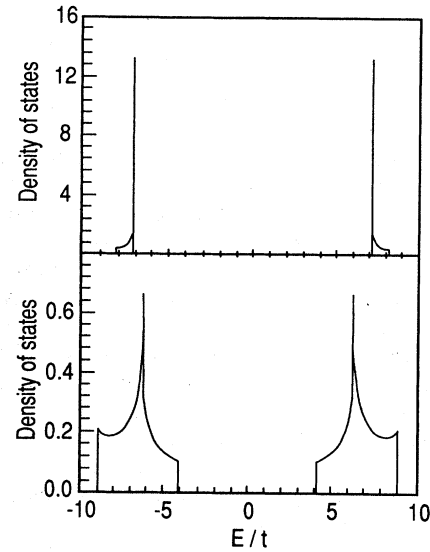


FIG. 3. The quasiparticle density of states per site in units t^{-1} at $U=15$ and $\delta=0$ (upper figure) and $\delta=0.1$ (lower figure) exhibiting the rapid expansion of the band with doping.

effect, lending support to the existence of at least local spiral order. The shifting of Q implies that hole pockets will appear slightly away from $(\pi/2, \pi/2)$. It is difficult to account for this broadening by a rigid-band approximation. If one interprets the upper band as the unfilled Cu d^{10} band, then this broadening can also be seen in inverse photoemission experiments. We also note that from Fig. 2(b) it is clear that Fermi-surface crossings should be observed both along Γ -S and Γ -X directions.¹⁴ The inclusion of the oxygen bands is necessary for detailed comparison with photoemission experiments.

Following Kohn,^{7,8} we have calculated a stiffness constant which measures the response of the system to an electromagnetic field. The stiffness constant Υ is defined

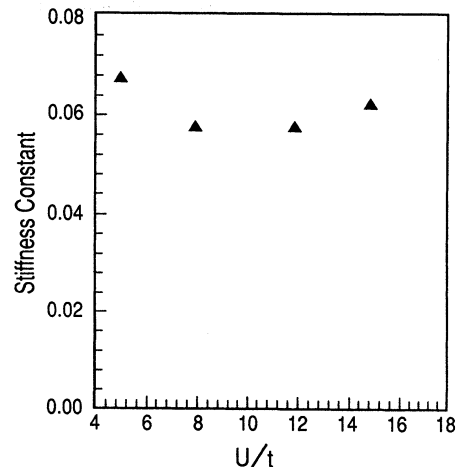


FIG. 4. The stiffness constant defined in Eq. (4) at $\delta=0.1$ as a function of U in the diagonal spiral phase.

as

$$Y = \frac{1}{2} (a^2/V) \left[-\langle \hat{T}_x \rangle - 2 \sum_{n \neq 0} \frac{|\langle 0 | \hat{j}_x | n \rangle|^2}{E_n - E_0} \right], \quad (4)$$

where $\hat{T}_x = -2t \sum_{k\sigma} \cos(k_x a) c_{k\sigma}^\dagger c_{k\sigma}$ is the kinetic-energy operator along the x axis and $\hat{j}_x = 2t \sum_{k\sigma} \sin(k_x a) c_{k\sigma}^\dagger c_{k\sigma}$. Y is a measure of how good a metal the system is, and vanishes for an insulator. It is easily shown that $\lim_{\omega \rightarrow 0} [\omega \sigma''(\omega)] = 2(e^2/\hbar^2)Y$ where σ'' is the imaginary part of the frequency-dependent conductivity. We find that in the diagonal spiral the stiffness constant vanishes nonlinearly with δ as $\delta \rightarrow 0$. We show a plot of Y as a function of U for $\delta=0.1$ in Fig. 4. Note the initial decrease and subsequent increase as a function of U ; as the system approaches the ferromagnetic state it becomes a better metal. It has the least metallic characteristics at intermediate U . An effective plasma frequency that characterizes the low-frequency properties ω_p^{*2} can be defined as $\omega_p^{*2} = 8\pi(e^2/d)Y$ where d is the interplanar spacing, and at $\delta=0.15$ this has a value of $2.75(\text{eV})^2$ if we assume an effective value of 0.5 eV for t . We have also calculated the effective plasma frequency which is determined by the f sum rule:¹⁵ $\omega_p^2 = -(4\pi^2 e^2 a^2 / \hbar^2 V) \langle T_x \rangle$. For large U , in the classical Néel state $\langle -T_x \rangle$ has the value $(\pi^2/2)(t/U)$. The deviations with doping are quan-

titatively small. We have also computed the number of doubly occupied sites to be $\frac{1}{4}(1-\delta)^2 - b_0^2$ and find that it decreases linearly with δ . We have not extended these calculations to values of δ larger than those considered here since particle-hole excitations of the holon Fermi sea—that destroy ferromagnetism and restore the Luttinger-Fermi surface¹⁶ at very large values of U and for large δ —are absent in this calculation.

It is also worth pointing out that effects due to the interaction between fluctuations of the spiral order parameter and the doubly occupied site-state and holon quasiparticles in the spiral metallic phase can, in principle, destroy the long-range spiral order, leaving behind just short-range spiral correlations. A precise elucidation of the phase diagram requires a careful calculation of the fluctuation effects for intermediate values of U/zt .

We are grateful to the Ohio Supercomputer Center and the Alabama Supercomputer Center for granting Cray computer time. C.J. acknowledges financial support from the National Science Foundation (Grant No. NSF-DMR 8451911). The research of S.S. was supported in part by a grant from the U.S. Department of Energy—Basic Energy Sciences, Division of Materials Research and the Cray Research Corporation. H.R.K. thanks P. W. Anderson for several stimulating discussions.

¹D. R. Penn, Phys. Rev. **142**, 350 (1965).

²B. I. Shraiman and E. D. Siggia, Phys. Rev. Lett. **62**, 1564 (1989).

³C. Jayaprakash, H. R. Krishnamurthy, and Sanjoy Sarker, Phys. Rev. B **40**, 2610 (1989).

⁴D. Yoshioka, J. Phys. Soc. Jpn. **58**, 1516 (1989).

⁵H. R. Krishnamurthy, C. Jayaprakash, S. Sarker, and W. Wenzel, Phys. Rev. Lett. **64**, 950 (1990).

⁶H. J. Schulz, Phys. Rev. Lett. **64**, 1445 (1990).

⁷W. Kohn, Phys. Rev. **133**, A171 (1964).

⁸B. S. Shastry and B. Sutherland, Phys. Rev. Lett. **65**, 243 (1990).

⁹W. Wenzel, C. Jayaprakash, H. R. Krishnamurthy, and S.

Sarker (unpublished).

¹⁰Y. Nagaoka, Phys. Rev. **147**, 392 (1966).

¹¹J. E. Hirsch, Phys. Rev. B **31**, 4403 (1985).

¹²Note that as $U \rightarrow 0$ the value of $(t/T)_{\text{eff}}$ can be argued to be nonvanishing in contrast to naive expectations. At half filling, the effective hopping parameter is the curvature of the lower Hubbard band while the effective exchange constant is determined by the gap. This leads to a finite value of t/J as $U \rightarrow 0$.

¹³J. Allen *et al.*, Phys. Rev. Lett. **64**, 595 (1990).

¹⁴J. C. Campuzano *et al.*, Phys. Rev. Lett. **64**, 2308 (1990).

¹⁵P. F. Maldague, Phys. Rev. B **16**, 2437 (1977).

¹⁶B. S. Shastry, H. R. Krishnamurthy, and P. W. Anderson, Phys. Rev. B **40**, 2375 (1990).